

Conformal Coating of Nanoparticles Using Atomic Layer Deposition in a Fluidized Bed Reactor

*Luis F. Hakim, Julie L. Portman, Michelle D. Casper, Alan W. Weimer**
Department of Chemical and Biological Engineering, University of Colorado, Engineering Center, ECCH 111,
Campus Box 424, Boulder, CO 80309, USA

Prepared for presentation at the 2004 AIChE Annual Meeting, Austin
Copyright © Luis F. Hakim, Julie L. Portman, Michelle D. Casper, Alan W. Weimer

AIChE shall not be responsible for statements or opinions contained in papers or printed in its publications

Abstract

The fluidization behavior of a variety of ultrafine powders was studied at increased and reduced pressures. Characteristics of stationary and fluidizing agglomerates of nanoparticles were described as well as the dynamic behavior of agglomerates during fluidization. The effect of different particle interactions such as adhesion, liquid bridging and electrostatic on various fluidization parameters was studied. It was found that when interparticle forces are reduced, minimum fluidization velocity (U_{mf}) and agglomerate size decrease and bed expansion increases. The fluidization characteristics were found to be mainly controlled by characteristics of agglomerates such as size and density. Modification in the fluidization behavior can be obtained by altering the surface chemistry of ultrafine particles. Coated particles via Atomic Layer Deposition (ALD) showed lower minimum fluidization velocity due to weaker interparticle attractions. It was also found that application of mechanical vibration to the fluidized bed reduces the agglomerate size and improves the fluidization quality.

Keywords: Fluidization, nanoparticles, agglomeration, vibration, vacuum, surface modification

1. Introduction

Fluidization of fine particles has been applied to several operations such as coating, separations, drying, granulation, crystallization, heat transfer and several chemical reactions [1-12]. More recently, increasing interest has been given to fluidization of nanoparticles. These are commonly defined as primary particles with dimensions less than 100 nanometers. Nanoparticles are known for offering the possibility to create novel materials by controlling properties such as morphology, spatial arrangement, size, surface chemistry and composition at the nano-scale. Therefore, processing of nanoparticles in a fluidized bed is an operation that will continue to grow in importance.

Due to strong cohesive forces, fluidization of ultrafine particles is characterized by agglomeration [13-17]. Properties of agglomerates, rather than those of primary particles, usually determine the fluidization behavior of ultrafine particles. A combination of various

* Corresponding author. Tel +1-303-492-7471; fax: +1-303-492-4341
E-mail address: alan.weimer@colorado.edu (A.W. Weimer).

interparticle forces such as London-Van der Waals, electrostatic interactions and liquid bridging may occur in a fluidized bed. These forces could form structures with such a high strength that fluidization is not possible, a typical behavior of type C particles in the Geldart classification [18]. Different systems that provide external agitation to the bed, such as sound and mechanical vibration have been applied in order to improve the quality of fluidization of ultrafine particles [3, 19-24].

The effect of pressure on the fluidization behavior of fine particles has also been extensively studied. A wide range of behaviors has been observed by several researchers. Sidorenko and Rhodes [25] found that minimum fluidization velocity of Geldart type B particles is slightly decreased for increasing pressures and was independent of pressure for Geldart A particles. Li and Kuipers [26] predicted that elevated pressures result in a more homogeneous flow pattern that reduces the minimum fluidization velocity and shortens the bubble regime. Llop et al. observed that minimum fluidization velocity increased with reducing pressure [27] and that slugging behavior occurs, progressively decreasing the quality of fluidization [28]. Similar trends in the fluidization velocity at low pressures were observed by Kozanoglu et al. [29] with no noticeable effect on the bed voidage.

Fluidization of nanoparticles is controlled by a combination of operating conditions, such as pressure, and intrinsic properties such as particle interactions. Even though many aspects of the fluidization of nanoparticles have been investigated individually, few works have focused on studying multiple factors simultaneously. The present work performs an inclusive study of the agglomeration of nanoparticles and the influence of different interparticle forces and its correlation to fluidization at reduced and increased pressures.

2. Experimental

The fluidization behavior of a variety of ultrafine powders was studied. Experiments were performed at pressures above and below atmospheric pressure. Both visual and instrumental determinations of the minimum fluidization velocity were carried out. An illustration of the experimental setup is shown in Fig. 1a.

For the visual experiments, two glass reactors were used. For runs at increased pressure a borosilicate glass reactor, 1-m height and 4-cm diameter, was used. The distributor plate in this reactor is constructed of coarse porous glass 30 cm from the bottom of the tube.

Visual experiments at reduced pressure were performed using a Pyrex™ tube, 92-cm height and 4.6-cm diameter with a glass-metal transition and a metal flange that contains the distributor plate. The distributor is porous metal with a mean pore size of 20 μm. The path inside the porous disc is highly tortuous preventing any nanoparticles from crossing the disc thickness.

A stainless steel column is utilized for the instrumental studies of fluidization. This column is 75 cm long and 4.6 cm in inside diameter. The distributor is also porous metal with a mean pore size of 20 μm. The columns are then attached to a second stainless steel piece 110 cm long and 4.6 cm in diameter.

A porous metal filter is used in the system to keep all the particles inside the reactor at all times. This 316L stainless steel element is 1.9 cm in outside diameter, 15.24 cm long and has a 0.5 μ m pore size. It is attached to the inside cap of the fluidization columns. Even though its pore diameter is larger than the primary particles, all the powders studied in this work fluidize in the form of aggregates that are several microns in size thus all particles remain inside the reactor during the experiment.

The fluidization system has capabilities for operating at reduced pressures and on mechanical vibration mode. Reduced pressure is achieved by using an Alcatel 2063 vacuum pump. The pressure inside the fluidization column is controlled by varying the opening of a Nupro[®] LD series diaphragm valve placed at the inlet of the vacuum pump. Vibration is added to the system through two vibro-motors from Martin Engineering with variable amplitude. Vibration frequency is controlled using an ACS 140 speed controller from ABB Drive and Power Products.

The vibro-motors are attached to a custom-built vibration platform. Four spring supports on this platform give homogeneous vertical vibration to the entire system. The fluidization column is attached to this platform via an aluminum mounting assembly. For details, see Fig. 1b.

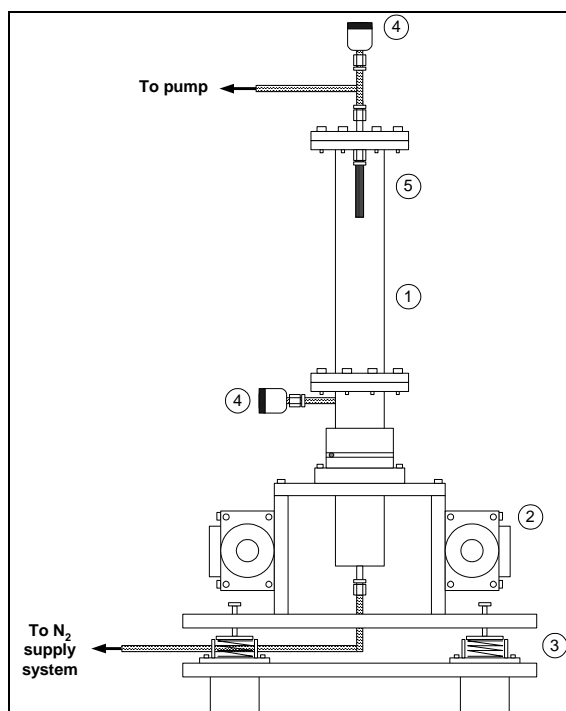


Fig. 1. (a) Schematic of fluidization apparatus: 1) Fluidization column, 2) vibro-motors, 3) spring supports, 4) pressure transducers, 5) sintered-metal filter. (b) System detail.

Nitrogen, from a high-purity source, is used as the fluidizing gas. Its flowrate is controlled by a MKS[®] 1179 series mass flow controller. Pressure gauges allow for measuring the pressure drop across the powder bed. MKS[®] 902 series piezo transducers are located right below the distributor plate as well as at the top outlet of the reactor.

The system is controlled and monitored using LabView[®]. A script records the pressure drop across the powder bed and allows for controlling the fluidizing gas flowrate and all the system valves.

The particles used in this study are hydrophilic Aerosil[®] silica particles types OX-50, 150 and 300 from Degussa; zirconia particles from NanoProducts Corp.; iron oxide (III) particles from Nanostructured and Amorphous Materials, and high-density polyethylene micron-size particles from Equistar. Physical properties of these powders are shown in Table 1.

	Silica Aerosil 300	Silica Aerosil 150	Silica Aerosil OX-50	Zirconia	Iron Oxide (III)	HDPE (with/without surface modification)
Primary particle size (nm)	7	14	40	26 ± 3	20-30	32 (μm)
BET Surface area (m²/g)	300 ± 30	150 ± 15	50 ± 15	40.9 ± 1.9	> 30	0.26
Density of primary particle (kg/m³)	2200	2200	2200	5890	5240	960
Bulk density of powder (kg/m³)	50	50	130	320	1500	510

Table 1. Physical properties of powders studied.

Fluidization of HDPE particles were studied before and after surface alteration. This modification was performed using an Atomic Layer Deposition process in a fluidized-bed reactor (ALD-FBR). Through this process, alumina nanolayers are conformally placed around the polymer particles. An approximate film thickness of 6 nm is expected on these particles after 50 ALD coating cycles. ALD-FBR is a very unique technique since it allows for placing films that are only a few nanometers in thickness. This process does not change the particle size distribution of the powder but modifies its surface properties. A more detailed description of this technique can be found in selected sources [30-34].

Visualization experiments were also performed in order to study the particles as they fluidize. Using a technique called Particle/Droplet Image Analysis (PDIA), a laser illuminates a region of interest from behind and shadow images of the aggregates are captured with a digital camera.

The selected region of interest is located near the upper surface of the fluidized bed, also known as the splash zone. This region is chosen because aggregates momentarily separate from the bed surface allowing its visual characterization. This region is located below the disengagement zone, so the level of elutriation is reduced. This assures that the size distribution of the visualized aggregates is representative of the one in the bed.

The PDIA system used was the Oxford Laser VisiSizer™. The laser (model HSI1000) provides pulses of infrared light at 805 nm. The laser system was coupled with a monochrome digital camera (Kodak Mega-Pixel Model ES1.0) with a standard silicon charge-coupled device sensor.

The laser and camera are triggered so that a single laser pulse freezes the motion of the agglomerates during each frame capture. The maximum analysis rate of the system is 30 frames per second. The pixel area of the particle aggregates is then measured and a special calibration of the system allows the equivalent aggregate diameter to be reported. Different lens magnifications will represent different field of views from which the size of the aggregates can be scaled.

In order to study the electrostatic effect on silica nanoparticles Kensington Anti-Static Spray was used to minimize interactions between the particles and the glass fluidization column.

3. Results and discussion

3.1 Agglomeration behavior of nanoparticles

The fluidization performance of particles is strongly driven by their size, density and, in a lower magnitude, its shape. For particles under agglomeration conditions, the properties of agglomerates, and not the ones of primary particles, commonly determine the fluidization characteristics. Therefore, developing an understanding of the agglomeration of nanoparticles is a fundamental step in trying to predict their fluidization behavior.

Nanoparticles show special agglomeration characteristics due to their small size. At the nano-scale, adhesive forces, known as London-Van der Waals forces [35], start to become important and often equilibrate the inertia of the particles.

London-Van der Waals forces are originated by a temporal dipole character that particles show depending on different electronic configurations [36]. This results in a generalized attraction of particles. The attraction energy between particles is inversely proportional to the sixth power of the particle radius. Therefore, this interaction becomes very significant for nanoparticles and agglomeration is commonly observed.

The natural tendency for agglomeration of nanoparticles makes it difficult to find isolated primary nanosized particles in dry systems. Many techniques that study nanoparticles rely on the use of surfactants in order to overcome these surface interactions and disperse the particulate systems.

As nanoparticles agglomerate into bigger aggregates, the balance between the cohesive and the inertial forces in the particulate system changes. The different levels of this force balance give the nanoparticulate systems their unusual characteristics. Different arrangements of nanoparticles can be identified as the size of these aggregates grows from only a few nanometers to several hundreds of microns. This phenomenon is controlled mainly

by the primary particle size, shape and roughness as well as the tendency of the particles to show other surface effects such as liquid bridging and electrostatic interactions.

Agglomeration behavior of nanoparticles is also dependent on the flow conditions. The type of agglomerates formed when particles are subjected to a gas flow, such as fluidization, show different characteristics than those formed in quiescent conditions. During fluidization, agglomerates are subjected to collision events due to the high level of solids recirculation. These frequent collisions as well as the continuous flow of gas through the bed are the main cause for the formation of unique agglomerates. For simplicity purposes, we will refer to the latter as fluidizing agglomerates and as stationary agglomerates to those formed during stagnant conditions.

Using a laser imaging system described previously, fluidizing agglomerates can be studied in real time. This on-line technique shows critical advantages since the agglomerates can be observed and measured while they fluidize. This allows for studying the characteristics of agglomerates while they are still interacting with other agglomerates and while gas flows through the bed. Methods that measure the agglomerate size after the bed has defluidized cannot capture these individualities. This is important since during fluidization, processing aggregates achieve sizes which for highly cohesive particles may be different than the stationary aggregate size [37].

An image of fluidizing agglomerates of Aerosil® 300 silica nanoparticles is shown in Fig. 2. Even though the primary size of these nanoparticles is 7 nm, their fluidizing agglomerates are several microns in size. Sphericity of these agglomerates is approximately 0.5, as measured by the laser imaging system, and they appear to be loosely packed. When agglomerates become large, near the limit for short and long range interactions that is usually a few microns in size [38], their weight starts to overcome the cohesiveness and inertial forces become more and more predominant.

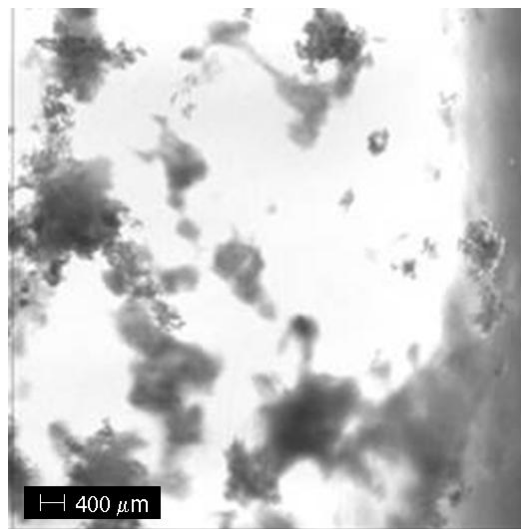


Fig 2. Fluidizing agglomerates of Aerosil 300 silica nanoparticles.

3.1.1 Dynamic agglomeration

Due to the relatively large size of the fluidizing agglomerates as well as the frequent collisions with other agglomerates, fluidizing agglomerates can show a dynamic behavior. This means that during fluidization, agglomerates of nanoparticles will continuously break apart and form again. This “dynamic equilibrium” between inertial and cohesive forces is one of the main effects that give nanoparticles such special fluidization characteristics.

Fig. 3a) and 3b) show two light microscope images of agglomerates of Aerosil® OX-50 silica nanoparticles. These agglomerates were obtained by drying separately three batches of nanoparticles red, green and white. These batches were fed into the fluidized bed with no previous mixing. The powders were fluidized together for 1 hr and a sample of the resulting powder was analyzed under the microscope. As it can be observed from the images, the agglomerates are formed by a composite of the three colors, meaning that the initial agglomerates broke apart and reform into these combined structures. This result offers qualitative evidence of the dynamic behavior of fluidizing agglomerates of nanoparticles.

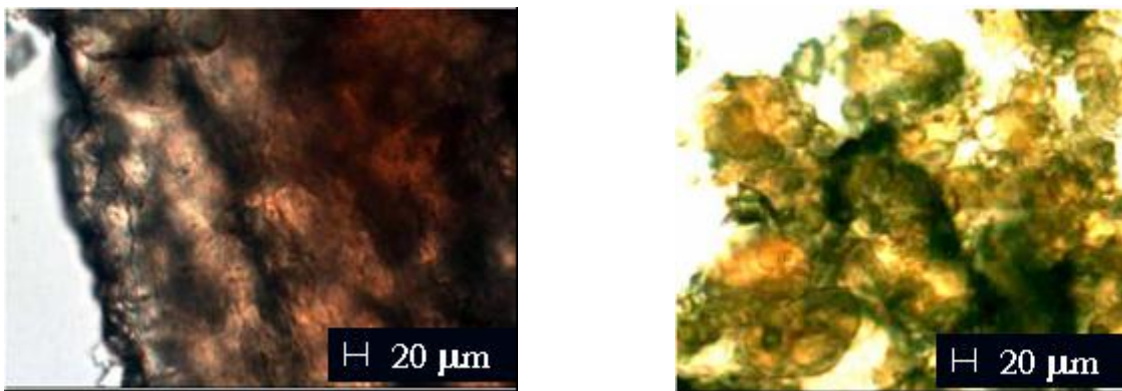


Fig 3 a) and b). Dynamic agglomerates of Aerosil OX-50 silica nanoparticles.

When nanoparticles are not subjected to any flow, stationary agglomerates will form due to various interparticle forces. However, the structure of stationary agglomerates will vary as the agglomerate size grows. This behavior was observed by Yao et al [39] using nanosized silica particles and was called multi-stage agglomeration (MSA).

At the smallest scale, nanoparticles will tend to arrange in chain-like structures that can achieve sizes of several hundreds of nanometers. These structures can be formed by hard or soft agglomerates. Hard agglomerates are commonly formed via coagulation of aerosol particles during the manufacturing process of nanoparticles. These agglomerates have a more rigid structure and are well identified for showing sintered areas in the contact points between nanoparticles. On the other hand, soft agglomerates are only maintained together due to London-Van der Waals forces. These agglomerates can be commonly broken apart if external agitation is used. Fig. 4 a) shows a transmission electron micrograph of a structure formed by both hard and soft agglomerates of zirconia nanoparticles.

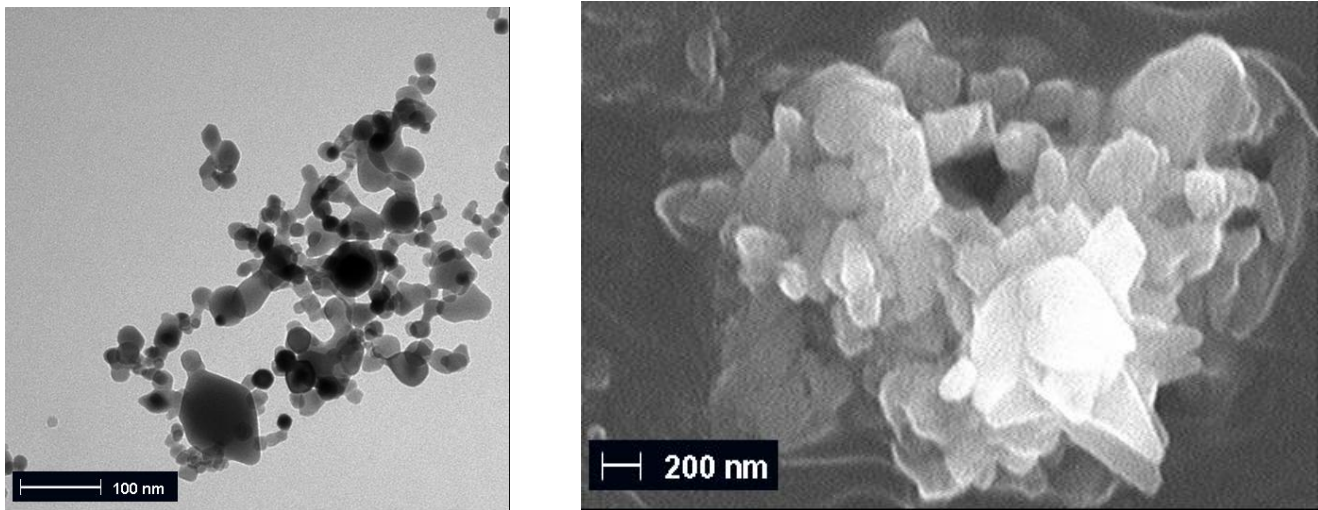


Fig. 4. a) TEM image of a stationary agglomerate of zirconia nanoparticles. b) SEM image of a stationary agglomerate of silica nanoparticles.

As stationary agglomerates grow, due to their increased mass, their structure will become more compacted. As opposed to fluidizing agglomerates, stationary structures are subjected to packing conditions during handling and storage. Additionally, atmospheric humidity will transfer moisture to the powder forming liquid bridges between nanoparticles. These conditions generate bigger, harder agglomerates with high stability. Fig 4 b) shows a scanning electron micrograph of a larger stationary agglomerate of silica Aerosil[®] OX-50 nanoparticles.

Flow conditions must be taken in account when studying agglomerates of nanoparticles. As their structures are affected by gas flow, recirculation and frequent collisions, the properties of fluidizing and stationary agglomerates may be very different.

3.2 Fluidization at increased pressure

The effect of interparticle forces on fluidization parameters was studied at increased pressure. Nanosized Aerosil[®] silica particles have special features that make them unique for understanding fundamental principles in fluidization processing. The most attractive characteristic of these particles is the existence of multiple interparticle forces that may or not be relevant depending on the selected operating conditions.

London-Van der Waals attractions originate solely due to the small size of particles. As it has been studied in previous works [20, 36, 40, 41], attractions of this type start to be important near the micron-sized range. London-Van der Waals forces become stronger as the particle size decreases, thus for nanosized particles, this effect is usually very strong.

Originated during the manufacturing process, siloxane (-Si-CH₃) and silanol (-Si-OH) groups can be found on the surface of Aerosil[®] particles [42]. These chemical groups give the particles the tendency to acquire a negative triboelectric charge. This phenomenon may create two possible effects. On one hand, repulsions between particles may exist due to the negative charge on their surface. On the other hand, due to a localized positive charge throughout the

glass, attractions may exist between the particles and the walls of the fluidization column. In this work, only the latter effect was studied.

The last type of interparticle interactions studied is liquid bridging. Aerosil® silica particles type OX-50, 150 and 300 show a hydrophilic behavior due to the silanol groups found on their surface. This again may generate interactions among particles or between the particles and the column walls, depending on the conditions of humidity during operation.

3.2.1 Effect of interparticle forces

Different operating conditions were used during the fluidization experiments to investigate the effect of interparticle forces on the fluidization behavior. Experiments were carried out varying the use of an anti-static surfactant and heat to remove moisture from the particles, the combination of both aids and its absence. Parameters such as the minimum fluidization velocity (U_{mf}), bed expansion, average aggregate size and sphericity were measured.

For this set of experiments, powders were previously sieved using a MESH 40 tray (< 420 μ m). This operation intends to eliminate large stationary agglomerates formed during storage. Drying of particles was performed at atmospheric pressure and 130 °C for 2 hours in a horizontal furnace. The anti-static surfactant was applied to the internal walls of the fluidization column and let dry at room temperature.

It was observed, as seen on Fig. 5, that the minimum fluidization velocity varied as the different fluidization aids were used. The three nanopowders followed similar trends. The minimum fluidization velocity when no aid was used was always the highest. A reduction in U_{mf} was observed when the anti-static surfactant and heat were used individually. This shows that both electrostatic interactions and capillary forces due to liquid bridging have an effect on the minimum fluidization velocity.

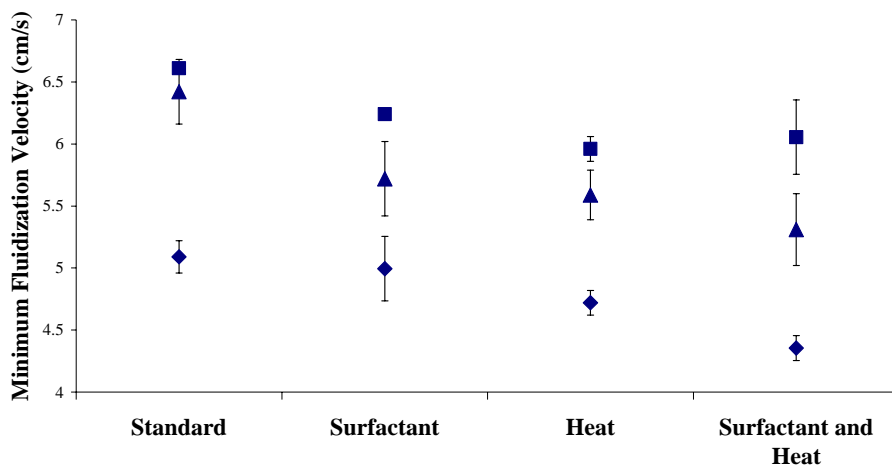


Fig. 5. Minimum fluidization velocity of silica nanoparticles at different operating conditions. Aerosil 300 (■), 150 (▲), OX-50 (◆)

Results for the bed expansion are shown in Fig. 6. For all the powders, the bed expansion increases as the interactions among particles (liquid bridging) and with the glass column walls (electrostatic) are reduced.

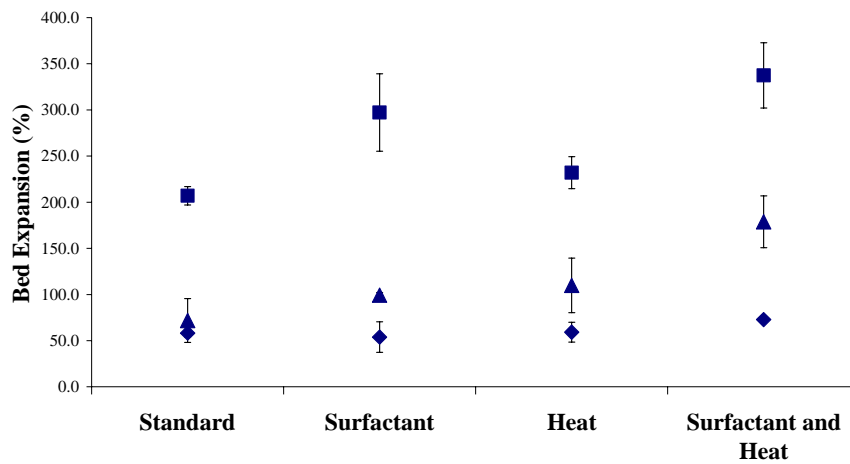


Fig. 6. Bed expansion of silica nanoparticles at different operating conditions. Aerosil 300 (■), 150 (▲), OX-50 (◆)

The fact that using an anti-static surfactant modifies U_{mf} and the bed expansion shows that there are indeed interactions between the walls of the column and the bed of particles. Whether or not wall-to-particle interactions should be included as an element of the force balance in a fluidized bed has remained a controversial issue. If this effect was unrelated to the fluidization of particles, there would be no change in the fluidization characteristics when interactions between the walls and the particles are modified.

As it has been considered by other authors [40, 43, 44], an expanded fluidized bed maintains its mechanical stability through a network structure, linking all the particles in the bed. This chain-like structure extends to the walls of the bed through the contact points between the walls and the network of particles. At the onset of fluidization, the upward force exerted by the gas has to overcome not only the weight of the bed of particles but also the frictional forces between the bed and the walls of the column. If frictional forces between the bed and the walls are reduced, lower minimum fluidization velocities and higher bed expansions would be expected. This explains why wall-to-particle interactions affect the fluidization behavior of the entire bed and should be included in the force balance for particles in a fluidized bed.

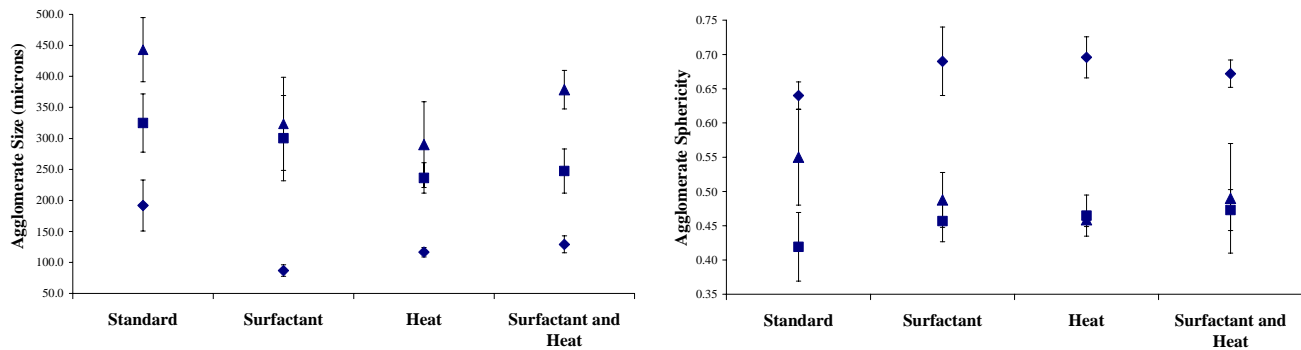


Fig. 7. Average agglomerate size and sphericity of silica nanoparticles at different operating conditions. Aerosil 300 (■), 150 (▲), OX-50 (◆)

Results for average agglomerate size and sphericity are shown in Fig. 7 a) and b). The fluidizing agglomerate size follows a similar behavior to that observed in the minimum fluidization velocity. As the attractive interparticle interactions are reduced, the tendency for agglomeration decreases forming smaller, lighter agglomerates. The sphericity of agglomerates does not seem to follow a clear trend. As mentioned before, the dynamic agglomeration behavior of nanoparticles constantly modifies the size and shape of agglomerates. This random behavior makes difficult to measure any effect that reduction of interparticle forces may have on the sphericity of fluidizing agglomerates.

These results suggest that minimum fluidization velocity is mainly controlled by the change in agglomerate size, as larger, heavier agglomerates require higher gas flowrates to fluidize. Additionally, the change in bed expansion is directly controlled by interactions within the fluidized bed (particle-particle and particle-wall-particle) due to reduced frictional forces. Overall, these observations show the importance of interparticle forces on the fluidization behavior of nanoparticles.

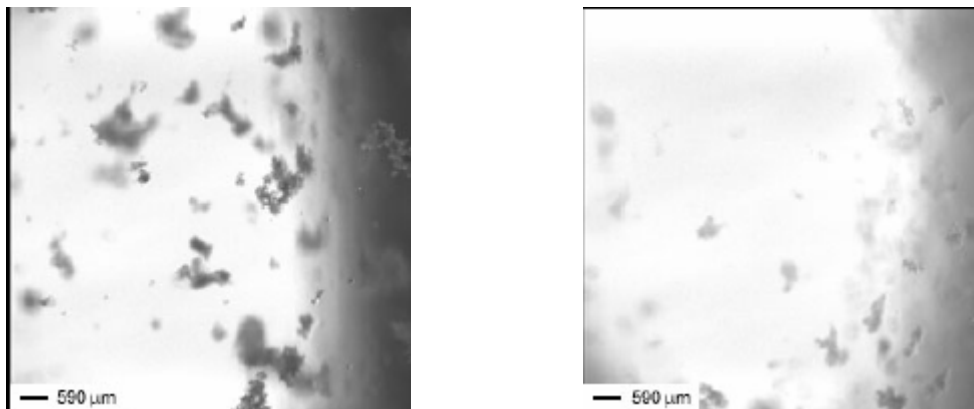


Fig. 8. Fluidizing agglomerates a) Standard run, b) Using dried particles and anti-static surfactant

Two images of fluidizing agglomerates of silica nanoparticles are shown in Fig. 8 a) and b). These pictures were taken using the high speed laser imaging system. It can be seen how the size of fluidizing agglomerates decreases when liquid bridging and electrostatic

interactions are reduced. No conclusions can be obtained on the effect of these interparticle forces on the sphericity of agglomerates. Formation of agglomerates follows a rather chaotic pattern due to constant recirculation, collision and breakage of agglomerates in the fluidized bed.

3.3 Fluidization at reduced pressure

Fluidization experiments were also performed at reduced pressure in order to study the effect on minimum fluidization velocity. Determination of U_{mf} was performed visually and instrumentally. Mechanical vibration was applied to the system in order to provide external agitation and to aid the fluidization of ultrafine particles.

Powders were previously sieved using a MESH 40 tray ($< 420 \mu\text{m}$) to eliminate large stationary agglomerates formed during storage. Particles were dried inside the fluidization column that was encased by a clamshell-type furnace (Fig. 1b). Drying of particles was performed for 2 hours at low pressure (200 mTorr) and $130 \text{ }^\circ\text{C}$ under a 15 sccm flowrate of Nitrogen. For fluidization experiments, pressure inside the reactor was varied by controlling the opening of a diaphragm valve placed at the inlet of the vacuum pump.

Visual determinations of U_{mf} were done using both the increasing and decreasing superficial gas velocity methods. Common discrepancies between these two methods can be explained by a hysteresis effect observed on particles that have been compacted to some extent [45-48]. In the experiments performed, the difference in the U_{mf} values obtained using these two methods is within the experimental error of this work.

Instrumental determination of U_{mf} was performed by measuring the pressure drop across the fluidized bed versus the superficial gas velocity. The minimum fluidization velocity is obtained by determining the value of gas velocity for which the pressure drop remains constant [49].

The results of the minimum fluidization velocity for all the powders studied are shown in Fig. 9. The plot shows the average of several experiments carried out with an average pressure of 16.5 Pa. The results obtained using both visual and instrumental measurements were very similar. In general, determining U_{mf} from a plot of pressure drop versus superficial gas velocity is more reliable, since all data come from instrumental measurements. In the visual experiment, defining when fluidization or defluidization occurs could be sometimes subjective leading to non-reproducible results.

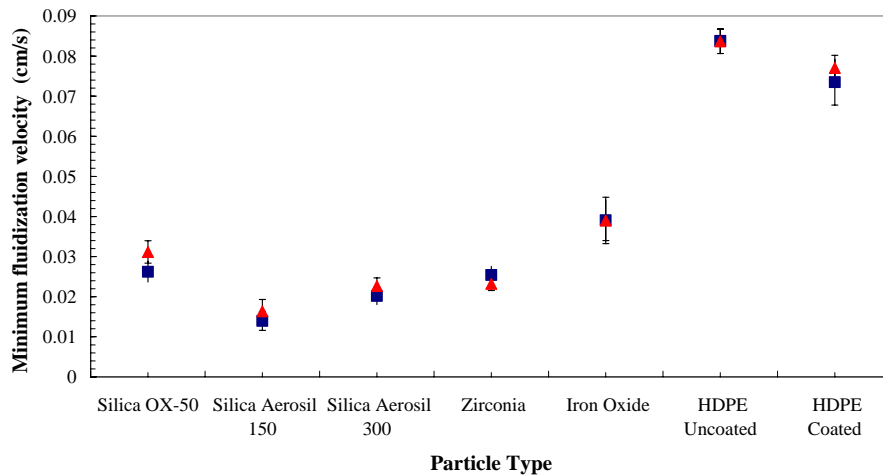


Fig. 9. Minimum fluidization velocities for visual (\blacksquare) and instrumental (\blacktriangle) determinations

The effect of particle size in the fluidization at reduced pressure was also studied. Aerosil[®] Silica particles types OX-50, 150 and 300 were fluidized and the column pressure was varied from 116 to 135 mTorr. As observed in Fig. 10, for this range of operating conditions no effect on U_{mf} was observed as the pressure was varied. It is important to note that, for all cases, the minimum fluidization velocity for Aerosil 300 (APS 7 nm) is larger than that for Aerosil 150 (APS 14 nm). This can be explained, as mentioned previously, by the fact that as particle size becomes very small, interparticle forces rapidly increase. For 7 nm particles, London-Van der Waals forces may be larger than for 14 nm particles. This large force would form bigger agglomerates that require a higher gas flowrate to fluidize.

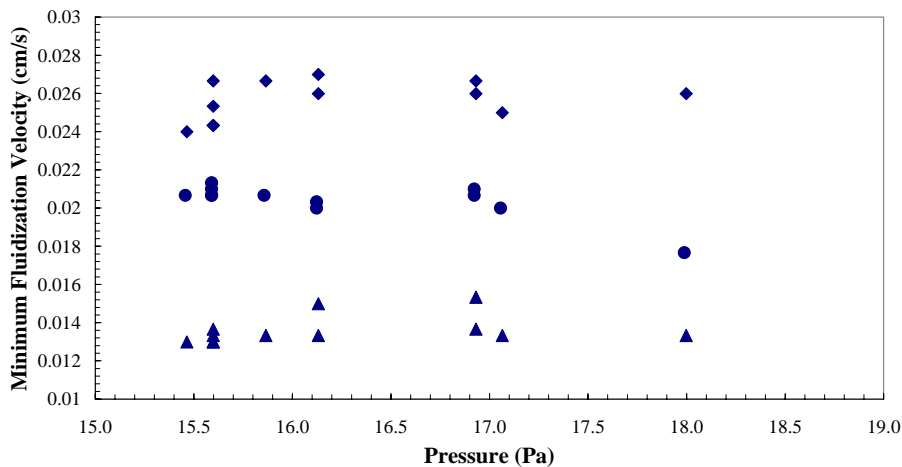


Fig. 10. Minimum fluidization velocity of silica nanoparticles at various low pressures. Aerosil OX-50 (\blacklozenge), 300 (\bullet) and 150 (\blacktriangle)

An additional example of the relevance that agglomerates characteristics have over the properties of individual particles is shown in Fig. 11. A plot of pressure drop across the bed versus superficial gas velocity is used to determine U_{mf} (marked with vertical lines) for both zirconia and iron oxide nanopowders. As observed, iron oxide particles show both a higher pressure drop as well as a higher minimum fluidization velocity relative to zirconia.

Even though these powders have a very similar average particle size (~ 25 nm) their fluidization plot looks very different. As observed in Table 1, the primary particle density for these powders is very similar. However, the bulk density, that is accepted to be corresponding to the density of fluidizing agglomerates and controlled by agglomeration mechanisms [14, 16, 39, 50] is more than four times greater for iron oxide. Particle-to-particle interactions may also differ for these materials. Nonetheless, the agglomerate density is a determining factor in the fluidization behavior of nanoparticles.

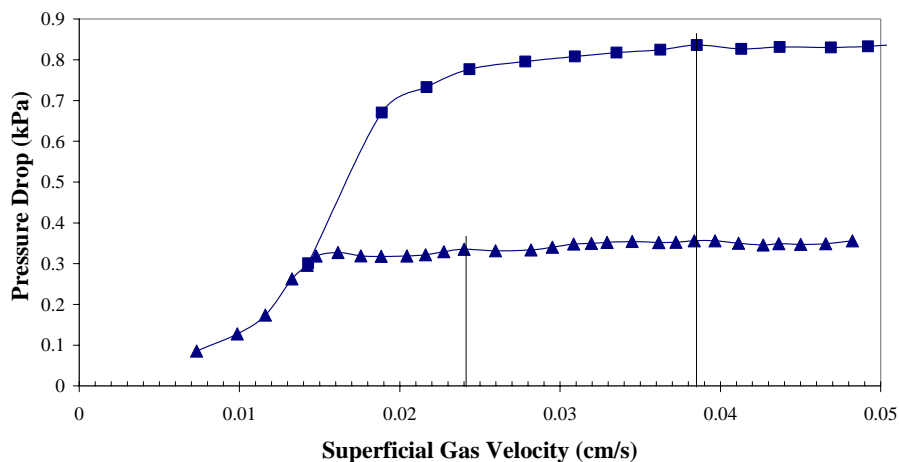


Fig. 11. Bed pressure drop vs. superficial gas velocity for zirconia (▲) and iron oxide (■) nanoparticles. Minimum fluidization velocities are marked with vertical lines.

The effect of surface chemistry on the fluidization behavior was also studied. High density polyethylene particles were coated with alumina nanolayers via Atomic Layer Deposition (ALD). By placing a thin film of a different material on the surface, particle-to-particle interactions are modified since a different Hamaker coefficient [36, 51] is now present between the surface of the particles.

As observed in Fig. 12, the minimum fluidization velocity for the coated particles is smaller for all the pressures studied. By changing the particle interactions, several mechanisms may exist. On one hand, it is possible that weaker cohesive forces between the coated polymer particles reduce the mechanical strength in the bed, requiring a lower gas flowrate to expand and fluidize the bed of particles. If interactions between alumina surfaces are weaker than those between polyethylene surfaces, it is also possible that coated particles are less likely to agglomerate, thus decreasing the minimum fluidization velocity. The nanolayers are so thin that the density of the material is not expected to change significantly [52]. Therefore changes in U_{mf} would be caused mainly by a change in the fluidizing agglomerate size.

Further work is currently being carried out in order to extend the understanding of this phenomenon and will be presented in a subsequent paper. By modifying the surface properties of ultrafine particles with ALD, improved fluidization characteristics may be obtained while keeping fundamental properties of the powder.

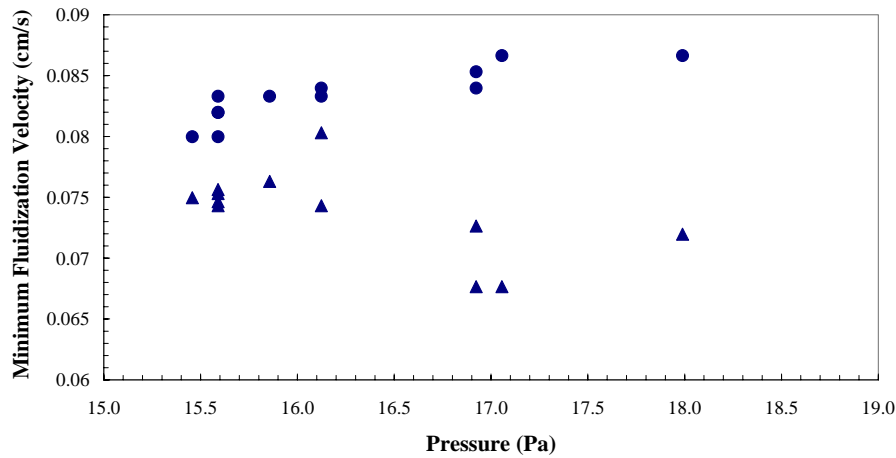


Fig. 12. Minimum fluidization velocity of coated (▲) and uncoated (●) HDPE at various low pressures.

Mechanical vibration was applied to the fluidized bed at reduced pressure in order to study the effect of an external perturbation on the aggregate size. As shown in Fig. 13, as the vibration frequency is increased, a sharp decrease in the aggregate size is observed. This can be explained because vibration generates a pressure fluctuation that is transferred to the bed via a gas gap [53]. This helps to partially overcome cohesive forces between primary particles and improve fluidization quality by reducing formation of channels and plugs.

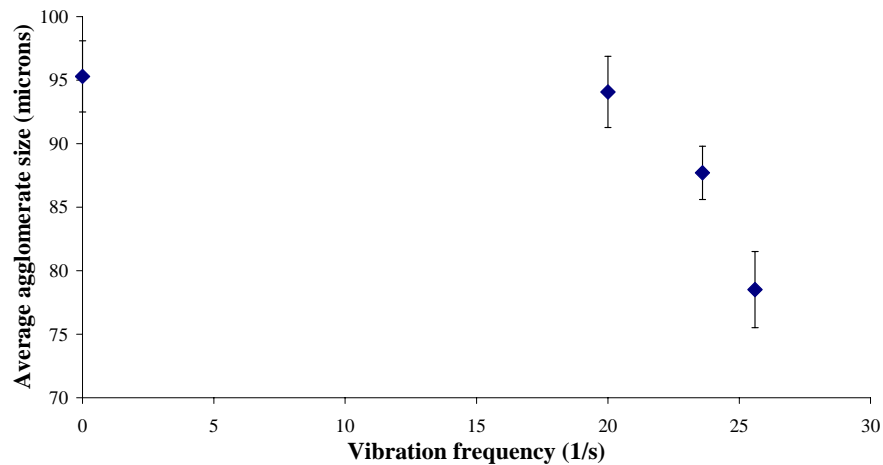


Fig. 13. Variation of aggregate size with vibration frequency for Silica Aerosil OX-50

Results shown in Fig. 13 were performed under vibration at reduced pressure (0.4 Torr). Particles were previously dried for this experiment. Whenever the vibration was stopped, the aggregate size remained essentially the same as in the experiments at increased pressure. This shows that even though decreasing pressure is expected to have an effect on minimum fluidization velocity [20, 25-28], it does not seem to affect the aggregation behavior.

For the range of reduced pressures studied, no effect was detected on the minimum fluidization velocity as the pressure was varied. However, for the runs at increased pressure, higher values of U_{mf} were observed. These results agree with the theory that as the pressure is increased, the mean free path of the gas molecules increases and the flow regime goes from viscous to slip and finally to a laminar state [20, 25-29]. Fluidized beds are usually operated in laminar or slip conditions, as very high flowrates are required to fluidize particles in molecular flow.

3.4 Conformal coating of nanoparticles

Silica and Zirconia nanoparticles were conformally coated using Atomic Layer Deposition. Previous works have focused on coating micron and submicron-sized particles [34]. This is the first attempt to coat bulk quantities of nanoparticles (less than 100 nm in size) using ALD in a fluidized bed reactor.

Fig. 14 shows a FTIR spectra of Silica Aerosil OX-50 particles processed under different conditions. The bulk alumina feature appears near 930 wavenumbers. An assesment of two operating conditions, continuous flow and static dose was performed. Continuous fow yield much better results due to improved gas-solids contacting. As observed, after 20 coating cycles, the spectra looks almost completely saturated. Equivalent results are shown in Fig. 15 for Zirconia nanoparticles.

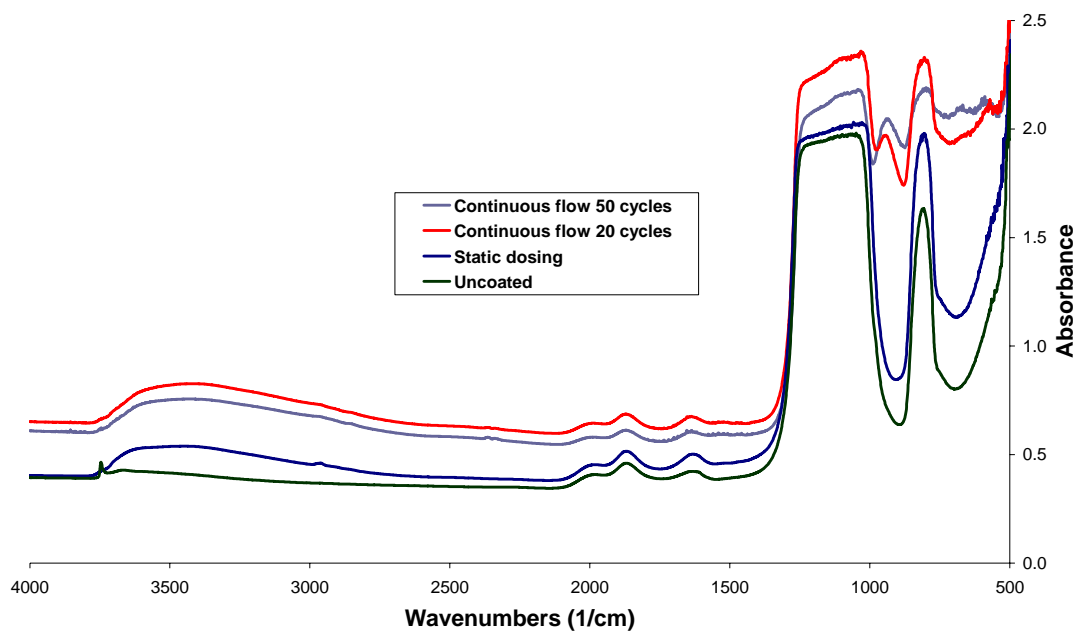


Fig. 14 FTIR spectra of alumina-coated Silica Aerosil OX-50 nanoparticles

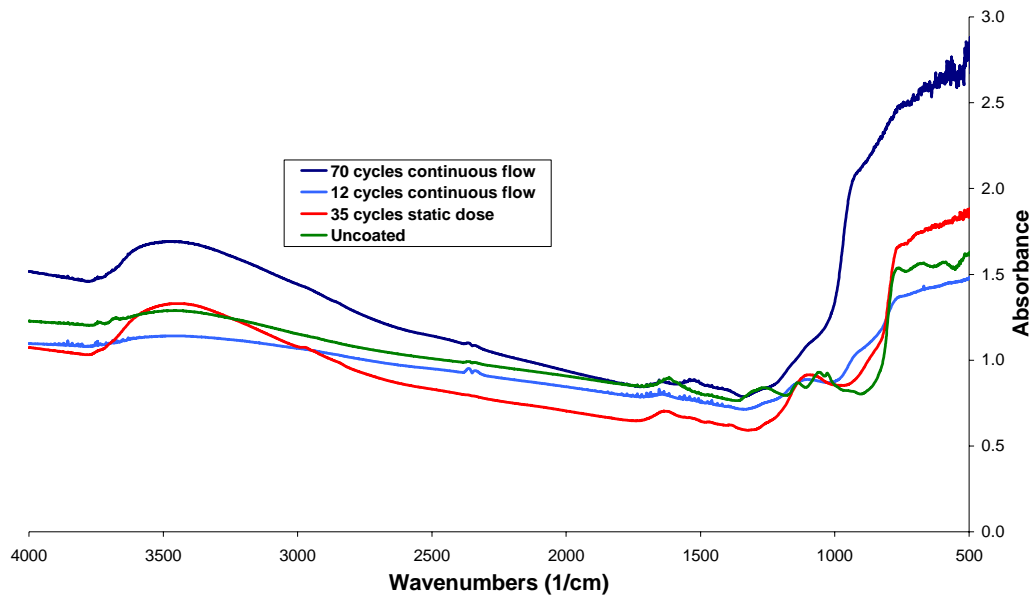


Fig. 15 FTIR spectra of alumina-coated Zirconia nanoparticles

Infrared spectroscopy proves bulk growth of alumina on the surface of nanoparticles. Additional parameters such as conformality and thickness uniformity can be tested via Transmission Electron Microscopy (TEM). Fig 16 a and b show TEM micrographs of zirconia nanoparticles coated with alumina nanolayers after 70 cycles. The average film thickness, measured visually, is 8.5 nm. ALD deposition of alumina has an optimum growth rate of 1.1 Angstrom per coating cycle [31]. This represents an expected thickness of 7.7 nm for 70 cycles that is very close to the calculated value. This result also proves that no CVD is occurring, since growth rates of films deposited via CVD are usually several nanometers per cycle.

Agglomeration of nanoparticles occur even for uncoated materials. It can be observed from the micrographs that individual nanoparticles are being conformally coated and that no additional aggregation is being created by the coating process. This is also proved by surface area analysis, where the value for the coated and uncoated particles remain statistically equal.

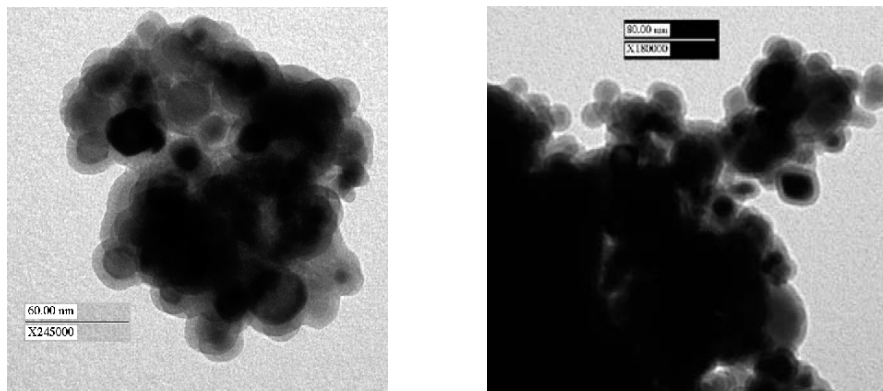


Fig. 16 TEM images of alumina-coated Zirconia nanoparticles

4. Conclusions

Nanoparticles naturally tend to agglomerate creating multiple-level structures due to multiple interparticle forces. Fluidizing agglomerates show a dynamic agglomeration behavior due to the flow of gas and constant collisions within the fluidized bed. Agglomerates under stagnant conditions show higher strength and stability than fluidizing agglomerates.

Interparticle forces such as cohesive London-Van de Waals, capillarity due to liquid bridging and electrostatic interactions play a key role in determining fluidizing parameters such as minimum fluidization velocity, bed expansion, agglomerate size and sphericity. In general, reduction of interparticle forces reduces U_{mf} and agglomerate size and allows for a higher bed expansion. No clear effect was detected on the sphericity of agglomerates. Particle-to-wall interactions participate in determining the fluidization characteristics of fine powders and should be included in the force balance for a fluidized bed.

Minimum fluidization velocity for nanoparticles slightly decreased as the pressure was increased. No main differences were detected between visual and instrumental determination of U_{mf} . Fluidization is mainly controlled by the agglomerate properties such as size and density, and not by individual particle characteristics. Surface modification by ALD can affect minimum fluidization velocity by changing particle-to-particle interactions. External mechanical vibration was successfully used to reduced the agglomerate size and improve the quality of fluidization.

Zirconia and Silica nanoparticles were conformally coated using Atomic Layer Deposition in a Fluidized Bed Reactor. Individual nanoparticles were coated and no further agglomeration is being produced due to the coating process.

Acknowledgments

The authors would like to thank the NSF-University of Colorado Research Experience for Undergraduates Program for supporting Julie Portman and Michelle Casper during the summers of 2003 and 2004 respectively.

We would to thank Joseph Spencer for providing the HDPE powder and performing the ALD surface modification, Degussa for providing the silica powders Aerosil[®] 150 and 300 and Kerr Corporation for providing the Aerosil[®] OX-50.

This work was funded by the National Science Foundation (Grant NER-0210670), the Department of Education GAANN Program in Functional Materials and the University of Colorado Engineering Excellence Fund.

References

1. Ishom, F., et al., *Problems in PFBC boiler (2): characterization of bed materials found in a commercial PFBC boiler at different load levels*. Fuel, 2004. **83**(7-8): p. 1019-1029.
2. Wu, Y., et al., *Induction charge on freely levitating particles*. Powder Technology, 2003. **135-136**: p. 59-64.
3. Mawatari, Y., et al., *Effect of particle diameter on fluidization under vibration*. Powder Technology, 2002. **123**(1): p. 69-74.
4. Jono, K., et al., *A review of particulate design for pharmaceutical powders and their production by spouted bed coating*. Powder Technology, 2000. **113**(3): p. 269-277.
5. Han, K.N., R. Sathyamoorthy, and M.C. Fuerstenau, *A study on the removal of fine particles by liquid fluidized beds*. International Journal of Mineral Processing, 1990. **29**(3-4): p. 279-287.
6. Pacek, A.W. and A.W. Nienow, *Fluidisation of fine and very dense hardmetal powders*. Powder Technology, 1990. **60**(2): p. 145-158.
7. Morooka, S., T. Okubo, and K. Kusakabe, *Recent Work On Fluidized-Bed Processing of Fine Particles As Advanced Materials*. Powder Technology, 1990. **63**(2): p. 105-112.
8. Zhao, G.Y., C.W. Zhu, and V. Hlavacek, *Fluidization of Micron-Size Ceramic Powders in a Small-Diameter Fluidized-Bed*. Powder Technology, 1994. **79**(3): p. 227-235.
9. Tardos, G. and R. Pfeffer, *Chemical reaction induced agglomeration and defluidization of fluidized beds*. Powder Technology, 1995. **85**(1): p. 29-35.
10. Litster, J.D. and R. Sarwono, *Fluidized drum granulation: studies of agglomerate formation*. Powder Technology, 1996. **88**(2): p. 165-172.
11. Janssen, L.P.B.M., et al., *The mechanical behaviour of vibrated, aerated beds of glass and starch powder*. Chemical Engineering Science, 1998. **53**(4): p. 761-772.
12. Hua, B. and C.Z. Li, *Production and characterization of nanocrystalline SnO₂ films on Al₂O₃ agglomerates by CVD in a fluidized bed*. Materials Chemistry and Physics, 1999. **59**(2): p. 130-135.
13. Arastoopour, H., C.S. Huang, and S.A. Weil, *Fluidization behavior of particles under agglomerating conditions*. Chemical Engineering Science, 1988. **43**(11): p. 3063-3075.
14. Chaouki, J., et al., *Effect of interparticle forces on the hydrodynamic behaviour of fluidized aerogels*. Powder Technology, 1985. **43**(2): p. 117-125.
15. Marinov, V., et al., *Ash agglomeration during fluidized bed gasification of high sulphur content lignites*. Fuel Processing Technology, 1992. **31**(3): p. 181-191.
16. Wang, Z., M. Kwauk, and H. Li, *Fluidization of fine particles*. Chemical Engineering Science, 1998. **53**(3): p. 377-395.
17. Kuwagi, K. and M. Horio, *A numerical study on agglomerate formation in a fluidized bed of fine cohesive particles*. Chemical Engineering Science, 2002. **57**(22-23): p. 4737-4744.
18. Geldart, *Types of Gas Fluidization*. Powder Technology, 1973. **7**(5): p. 285-292.
19. Zhu, C., et al., *Sound assisted fluidization of nanoparticle agglomerates*. Powder Technology, 2004. **141**(1-2): p. 119-123.
20. Wank, J.R., A.W. Weimer, and S.M. George, *Vibro-Fluidization of Fine Boron Nitride Powder at Low Pressure*. Powder Technology, 2001. **121**(2-3): p. 195-204.
21. Wang, T.-J., et al., *Energy transfer mechanism in a vibrating fluidized bed*. Chemical Engineering Journal, 2000. **78**(2-3): p. 115-123.
22. Marring, E., A.C. Hoffmann, and L. Janssen, *The Effect of Vibration On the Fluidization Behavior of Some Cohesive Powders*. Powder Technology, 1994. **79**(1): p. 1-10.
23. Leu, L.-p., J.-t. Li, and C.-M. Chen, *Fluidization of group B particles in an acoustic field*. Powder Technology, 1997. **94**(1): p. 23-28.

24. Russo, P., et al., *The influence of the frequency of acoustic waves on sound-assisted fluidization of beds of fine particles*. Powder Technology, 1995. **82**(3): p. 219-230.
25. Sidorenko, I. and M.J. Rhodes, *Influence of pressure on fluidization properties*. Powder Technology, 2004. **141**(1-2): p. 137-154.
26. Li, H., et al., *The cluster size distribution and motion behavior in a fast fluidized bed*. Powder Technology, 1995. **84**(3): p. 241-246.
27. Llop, M.F., et al., *Fluidization at vacuum conditions. A generalized equation for the prediction of minimum fluidization velocity*. Chemical Engineering Science, 1996. **51**(23): p. 5149-5157.
28. Llop, M.F. and N. Jand, *The influence of low pressure operation on fluidization quality*. Chemical Engineering Journal, 2003. **95**(1-3): p. 25-31.
29. Kozanoglu, B.U., et al., *Hydrodynamics of large particle fluidization in reduced pressure operations: an experimental study*. Powder Technology, 2002. **125**(1): p. 55-60.
30. Ferguson, J.D., A.W. Weimer, and S.M. George, *Atomic layer deposition of boron nitride using sequential exposures of BCl₃ and NH₃*. Thin Solid Films, 2002. **413**(1-2): p. 16-25.
31. Ferguson, J.D., A.W. Weimer, and S.M. George, *Atomic Layer Deposition of Al₂O₃ and SiO₂ on BN Particles Using Sequential Surface Reactions*. Applied Surface Science, 2000(162/163): p. 280-292.
32. Wank, J.R., et al., *Coating Fine Iron Particles with an Oxidation-Resistance Alumina Nanolayer Using ALD in a Fluidized Bed Reactor*, in *Fluidization XI, Engineering Foundation*. 2003.
33. Wank, J.R., S.M. George, and A.W. Weimer, *Coating Fine Nickel Particles with Al₂O₃ utilizing and Atomic Layer Deposition Fluidized Bed Reactor*. J. Amer. Ceram. Soc., 2003.
34. Wank, J.R., S.M. George, and A.W. Weimer, *Nanocoating individual cohesive boron nitride particles in a fluidized bed by ALD*. Powder Technology, 2004. **142**(1): p. 59-69.
35. Hamaker, H.C., *The London-Van Der Waals attraction between spherical particles*. Physica, 1937. **4**: p. 1058.
36. Visser, J., *Vanderwaals and Other Cohesive Forces Affecting Powder Fluidization*. Powder Technology, 1989. **58**(1): p. 1-10.
37. Zhou, T. and H. Li, *Effects of adding different size particles on fluidization of cohesive particles*. Powder Technology, 1999. **102**(3): p. 215-220.
38. Israelachvili, J.N., *Intermolecular and Surface Forces*. 9 ed. 2002, San Diego: Academic Press. 450.
39. Yao, W., et al., *Fluidization and agglomerate structure of SiO₂ nanoparticles*. Powder Technology, 2002. **124**(1-2): p. 152-159.
40. Jaraiz, E., S. Kimura, and O. Levenspiel, *Vibrating Beds of Fine Particles - Estimation of Interparticle Forces From Expansion and Pressure-Drop Experiments*. Powder Technology, 1992. **72**(1): p. 23-30.
41. Iwadate, Y. and M. Horio, *Prediction of agglomerate sizes in bubbling fluidized beds of group C powders*. Powder Technology, 1998. **100**(2-3): p. 223-236.
42. Degussa, *Aerosil Fumed Silica Technical Information Brochure*. 2001: p. 4-29.
43. Mutsers, S.M.P. and K. Rietema, *The effect of interparticle forces on the expansion of a homogeneous gas-fluidized bed*. Powder Technology, 1977. **18**(2): p. 239-248.
44. Rietema, K., *Powders, what are they?* Powder Technology, 1984. **37**(1): p. 5-23.
45. Bi, H.T., J.R. Grace, and J. Zhu, *Propagation of pressure waves and forced oscillations in gas-solid fluidized beds and their influence on diagnostics of local hydrodynamics*. Powder Technology, 1995. **82**(3): p. 239-253.
46. Gogolek, P.E.G. and J.R. Grace, *Fundamental hydrodynamics related to pressurized fluidized bed combustion*. Progress in Energy and Combustion Science, 1995. **21**(5): p. 419-451.

47. Polashenski, J., William and J.C. Chen, *Normal solid stress in fluidized beds*. Powder Technology, 1997. **90**(1): p. 13-23.
48. Rhodes, M.J., *Introduction to Particle Technology*, ed. Wiley. 1998, New York.
49. Kunii, D. and O. Levenspiel, *Fluidization Engineering*. 1969, New York: John Wiley and Sons. 534.
50. Zhou, T. and H. Li, *Force balance modelling for agglomerating fluidization of cohesive particles*. Powder Technology, 2000. **111**(1-2): p. 60-65.
51. Milling, A., P. Mulvaney, and I. Larson, *Direct Measurement of Repulsive van der Waals Interactions Using an Atomic Force Microscope*. Journal of Colloid and Interface Science, 1996. **180**(2): p. 460-465.
52. Wank, J.R., *Coating Particles with Alumina Nanolayers Utilizing Atomic Layer Deposition in a Fluidized Bed Reactor*, in *Chemical Engineering*. 2003, University of Colorado: Boulder.
53. Siebert, A.W., D. Highgate, and M. Newborough, *Heat transfer characteristics of mechanically-stimulated particle beds*. Applied Thermal Engineering, 1999. **19**(1): p. 37-49.